In Situ Investigations on Organic Foam Films Using Neutron and Synchrotron Radiation

Janine Etrillard,*,† Monique A. V. Axelos,‡ Isabelle Cantat,† Franck Artzner,† Anne Renault,† Thomas Weiss,§ Renaud Delannay,† and François Boué||

Groupe Matière Condensée et Matériaux, UMR CNRS 6626, Université de Rennes I, Campus de Beaulieu, 35042 Rennes Cedex, France, Unité de recherche Biopolymères, Interactions, Assemblages, INRA, BP 71627, 44316 Nantes Cedex 03, France, Laboratoire Léon Brillouin, UMR 12 CEA/CNRS, CE Saclay, 91191 Gif-sur-Yvette Cedex, France, and The European Synchrotron Radiation Facility (ESRF), 6 rue Jules Horowitz, BP 220, 38043 Grenoble Cedex 9, France

Received September 10, 2004. In Final Form: December 4, 2004

We report on small-angle neutron scattering (SANS) and X-ray scattering (SAXS) investigations of foam films stabilized by sodium dodecyl sulfate. Previous measurements on dry foams (Axelos, M. A. V.; Boué, B. *Langmuir* **2003**, *19*, 6598) have shown the presence of spikes in the two-dimensional scattering data which suggest that the incident beam is reflected on some film surfaces. The latter interpretation is confirmed by new neutron studies performed on ordered ("bamboo") foams which allow selection of single films. In the first case, we show that the spikes of the scattered intensity can be obtained by reflection on two parts of the foam, namely, the films and the Plateau borders. With synchrotron radiation, first observations of distinct interference fringes have allowed an accurate determination of the film thickness. A comparison with X-ray and neutron data is made, opening a general discussion about the capabilities of small-angle scattering techniques for studying the microscopic properties of foam films.

1. Introduction

In many industrial applications of foams, their macroscopic stability is of crucial importance: for instance in food manufacturing, firefighting, mineral flotation, decontamination of radioactive components, etc. The efficiency of foams is closely related to the structural and rheological properties of single foam films and to those of the network they form in real foams.[1] Most investigations are carried out on single plane-parallel films to study the interfacial properties such as the stabilizing surface forces via the disjoining pressure (thin film pressure balance[2]), the structure of Newton black films as revealed by X-ray reflectivity,[3−5] and the stratification in planar air/solution interfaces as studied by neutron reflectometry.[6] However, the behavior of a single liquid film does not seem sufficient to explain the behavior of the whole foam. The rupture of thin liquid films separating two adjacent cells (coalescence) is coupled to the drainage, governed by an evolution of the liquid fraction of the foam.[7] It will thus be useful to gain a direct insight into the films of a foam during its formation and destabilization.

Very recent small-angle neutron scattering (SANS) experiments, obtained in situ on three-dimensional aqueous foams stabilized by a surfactant, namely, sodium dodecyl sulfate (SDS), have provided information about their internal structure, from the scale of the liquid film thickness to the size of gas bubbles.[8] Isotropic as well as anisotropic scattering data have been collected for two kinds of foams: wet foams in the steady-state regime of constant gas bubbling and dry foams under free draining conditions. Reliable scattering spectra were obtained within a few minutes, even for very dry foams. All spectra have a basic $I(q) \sim q^{-4}$ (q, scattering vector) behavior on which a foam specific spectrum structure is superimposed. The q^{-4} decrease at low q can be interpreted in terms of a Porod law from which the average bubble size is determined for both wet and dry foams. For wet foams, the intensity is modulated at high q by the structural organization of the surfactants in the liquid fraction of the foam (micelles). Remarkably, for dry foams only, a spectrum structure associated with the typical film thickness also appears at intermediate q. This structure can be enhanced by using deuterated sodium dodecyl sulfate to suppress the micelle signal. Finally, measurements on dry foams have revealed spikes in the two-dimensional scattering data, suggesting that the incident beam is reflected on some bubble films.

We shall present here new SANS investigations on oriented and connected films in ordered (SDS) foams. The spikes remain unexplained in ref 8 but appear as promising to probe in situ the foam structure. The aim of this paper is thus to determine on a single film the origin of these spikes and their correlations with the film shape. We show that a single film can lead to a spike if its curvature is large enough. Similar spikes can also be attributed to Plateau borders, but in this case no oscillation is expected along the spike. This work is a new step to be able to quantitatively interpret the pattern obtained on a whole foam in the same experimental conditions. We check the

* To whom correspondence may be addressed. E-mail: janine.etrillard@univ-rennes1.fr.

† Groupe Matière Condensée et Matériaux, UMR au CNRS 6626, Université de Rennes I.

‡ Unité de recherche Biopolymères, Interactions, Assemblages, INRA.

§ The European Synchrotron Radiation Facility (ESRF).

|| Laboratoire Léon Brillouin, UMR 12 CEA/CNRS.

(1) Weaire, D.; Hutzler, S. *The Physics of Foams*; Clarendon Press: Oxford, U.K., 1999.

(2) Bergeron, V.; Claesson, P. M. *Adv. Colloid Interface Sci.* **2002**, *96*, 1.

(3) Bélorgey, O.; Benattar, J. J. *Phys. Rev. Lett.* **1991**, *66*, 313.

(4) Benattar, J. J.; Schalchi, A.; Bélorgey, O. *Phys. I Fr.* **1992**, *2*, 955.

(5) Sentenac, D.; Benattar, J. J. *Phys. Rev. Lett.* **1998**, *81*, 160.

(6) Ederth, T.; Thomas, R. K. *Langmuir* **2003**, *19*, 7727.

(7) Carrier, V.; Colin, A. *Langmuir* **2003**, *19*, 4535.

(8) Axelos, M. A. V.; Boué, F. *Langmuir* **2003**, *19*, 6598.

10.1021/la0477338 CCC: $30.25
Published on Web 02/10/2005

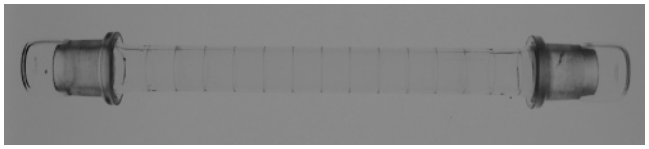

Figure 1. Photography of a bamboo structure with equally spaced transverse films.

coherence between the results obtained on a single film and the results in ref 8. After having described the experimental procedure, we shall emphasize some methodological aspects of the specular neutron reflectivity technique which require an unconventional use of a SANS spectrometer. A comparison with X-ray synchrotron results is made to validate some theoretical predictions. Some basic principles of specular neutron reflectivity are briefly recalled in the Appendix.

2. Experimental Procedures

As-received hydrogenated sodium dodecyl sulfate (SDS-h) and deuterated SDS (SDS-d) with an isotopic deuterium enrichment of 98% (Eurisotop) were used to prepare 12 g/L SDS solutions in 100% deuterated water. The difference in scattering length density $\Delta\rho^2$, the so-called contrast, is large both for SDS/D_2O ($\Delta\rho^2 = 35.74 \times 10^{20}$ cm^{-4}) and for D_2O/air ($\Delta\rho^2 = 40.26 \times 10^{20}$ cm^{-4}). Another possibility is to use the small value of the contrast between the surfactant and the solvent in the SDS-d/D_2O mixture ($\Delta\rho^2 = 0.148 \times 10^{20}$ cm^{-4}) to prevent the SDS structure (micelle signal) from being seen. The concentration of 12 g/L, which is beyond the critical micellar concentration value (cmc = 2.3 g/L), was chosen to ensure the foam stability and to facilitate the comparison of the present neutron scattering measurements with the previous ones.[8]

Instead of more classical bubbling procedures,[9,10] as used before[8] with the drawback of a need of large amounts of solutions, we have adapted to SANS a small container whose nozzle has the same diameter as the quartz cylindrical tube (1.4 cm diameter, 25 cm length). The liquid fraction, the flow rate, and the position of the end of the nozzle relative to the interface are important parameters to control the foam topology, the average bubble size, and the structure defined by the number of interconnected bubbles. For a bamboo structure of equally spaced transverse films (Figure 1), the end of the nozzle is just positioned at the gas/liquid interface. Once a foam is prepared, the tube is closed by quartz caps to prevent evaporation. The foam exhibits a high stability (lifetime up to 3 h). A sample environment (goniometer head) for transmission or reflectivity measurements has been built to control the translation or rotation of the tube. A single foam film is selected for the reflectivity measurements. For a horizontal tube orientation, films are nearly flat with Plateau borders (edges) whose thickness is variable with height vertically. When the tube is nearly vertical, both the drainage and the frequency of film ruptures increase.

SANS experiments were performed at the Orphée reactor of the Laboratoire Léon Brillouin (Saclay), on two different cold neutron spectrometers. The first set of measurements was performed on the PAXE spectrometer which is equipped with a XY detector of 64 × 64 cells of $s = 1 \times 1$ cm^2. The wavelength was 8 Å, and the sample−detector distance was $D = 4.5$ m. Collimation was achieved with a diaphragm of 7 mm put just before the sample. Using a SDS-h/D_2O foam, the measurement time was about 200 s, and data were not corrected (neutron beam transmission, incoherent scattering). The quartz tube contribution was neglected. The neutron and electronic background noise is only 7 counts per second (counts/s) for the whole detector (4096 cells). Additional measurements were done on the PAXY spectrometer, with a two-dimensional detector (128 × 128 cells of $s = 0.5 \times 0.5$ cm^2) offering a better resolution. The incident collimation was obtained from a first diaphragm of 4 mm and a second one of 19 mm (sample−detector distance $D = 6.7$ m), with a wavelength of 10 Å. For the second set of measurements, a SDS-d/D_2O foam was used with an exposure time of 500 s.

Small-angle X-ray scattering (SAXS) experiments have been performed at the high brillance ID-2 spectrometer at the ESRF (Grenoble, France). The operating beam energy was 12.5 keV, corresponding to a peak wavelength of 1 Å, with a cross section of 200 × 200 μm^2. The sample to detector distance was 1.232 m and the detector type used was an image intensified CCD camera (1024 × 1024 pixels, acquisition time of 10 ms). The solution used for this sample was also obtained by mixing 12 g/L SDS solution and pure water. To produce a foam, the solution was beaten stiffly and the foam is introduced in the quartz glass-capillary tube (purchased from Glas, diameter of 3 mm) by a syringe.

3. Results and Discussion

Previous SANS experiments performed on SDS aqueous foams[8] have revealed a progressive appearance of anisotropy in the scattering data when the drainage proceeds. When the foam becomes very dry, the scattering intensity is particularly high with good statistics in some angular sectors called "spikes". The origin of this scattering has been explained by Fresnel's reflectivity of the incident beam on some bubble films. In the present neutron scattering investigations, it was essential to choose an ordered foam to control the film orientation and therefore to confirm the previous interpretation based on a reflectivity assumption.

3.1. Spikes in the Neutron Scattering Pattern. An experiment performed with a disordered foam in a vertical tube produced a scattering pattern similar to that found with the PAXE detector (Figure 2a). Then we used a bamboo SDS-h/D_2O foam. Two kinds of patterns have been obtained: a circular intensity spot (Figure 2b, ∼7 cm diameter) and a distinct elongated spike shape, with a height of about 30 cm (Figure 2c). The intensity along the signal is masked in the middle by the beamstop (which avoids a saturation of the detector by the direct beam). The spot has been obtained for a tube placed vertically, which accelerates the liquid drainage, whereas spikes have appeared when the tube is horizontal and the Plateau border larger. The beam incidence angle on the films is almost identical in both situations because the rotation axis of the tube is along the beam. We thus attribute the spikes to the presence of large Plateau borders, in which almost all the water is trapped, as discussed below.

A brief outline of the theoretical background of the specular reflection of neutrons[11−14] is given in the Appendix.

3.2. Interpretation of the Spikes. In the case of a purely reflective situation, observing spikes instead of spots should be related with a wider distribution of orientation of the interface. The film is horizontal and the curvature due to its own weight can be estimated as follows: $4\gamma/R_f = gd\rho_w$ with $\gamma \approx 30$ mN/m the surface tension, R_f the film radius of curvature, g the gravity, $d \approx 20$ nm the film thickness, and $\rho_w \approx 1$ kg/L the water density. We get $R_f \approx 1 \times 10^3$ m, and the induced orientation variation of the film surface is $\delta\Theta = d_{tube}/(2R_f) \approx 1 \times 10^{-5}$ rad, which is much less than the incident beam divergence and therefore not observable.

Another origin of film orientation variation can be the Plateau borders, which connect here the thin film to the

(9) Weaire, D.; Hutzler, S.; Pittet, N. *Forma* **1992**, *7*, 259.
(10) Pittet, N.; Rivier, N.; D. Weaire, D. *Forma* **1995**, *10*, 65.
(11) Russel, T. P. *Materi. Sci. Rep.* **1990**, *5*, 171.
(12) Penfold, J.; Thomas, R. K. *J. Phys. Condens. Matter* **1990**, *2*, 1369.
(13) Daillant, J.; Gibaud, A. *X-ray and Neutron reflectivity*: *Principles and Applications*; Springer-Verlag: Telos, 1999.
(14) Nevot, L.; Croce, P. *Rev. Phys. Appl.* **1980**, *15*, 761.

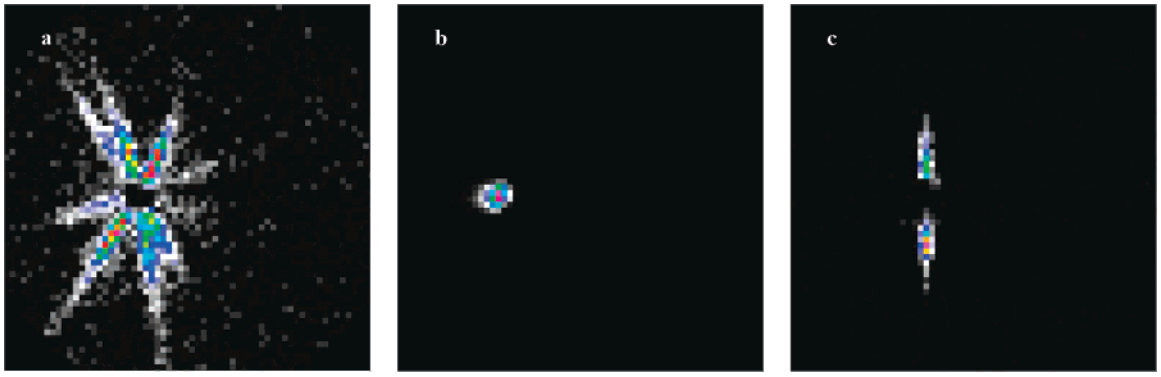

Figure 2. *XY* patterns of the intensity map on the two-dimensional detector (PAXE), from a disordered foam (a) or a bamboo foam (b, c). The q_0 varies from 0.005 to 0.056 Å^{-1}.

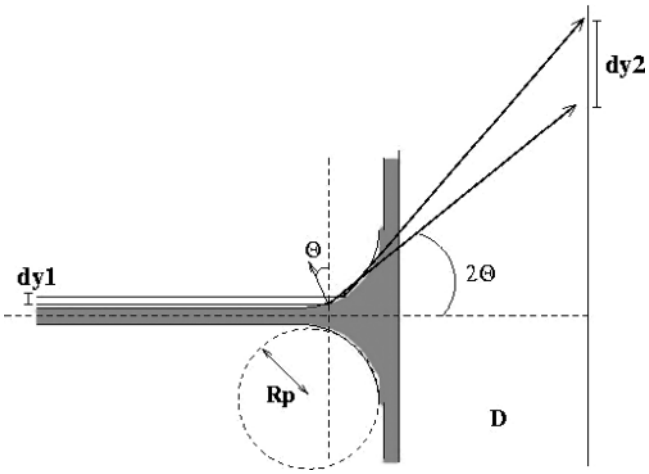

Figure 3. Schematic description of the neutron reflection on the Plateau border.

tube wall. Here the air/water interface makes a sharp rotation of $\pi/2$ on a very short distance of the order of the Plateau border size, typically 1 mm. We assume a purely reflective situation, with a reflectivity $R(\Theta)$ only depending on the incidence angle $\pi/2 - \Theta$. Since we consider Plateau borders, the thickness of the film can be considered as infinite. Using Figure 3, we predict the intensity on the spikes obtained for this geometry. The intensity at the position y_2 on the detector is given by $I(y_2) = I_0R(\Theta)\, dy_1/dy_2$ (I_0, incident intensity), the neutrons in the sheet (y_1, $y_1 + dy_1$) being deflected on the detector in the sheet (y_2, $y_2 + dy_2$), or transmitted. As $y_1 = R_p(1 - \cos\Theta) \approx R_p\Theta^2/2$ and $y_2 = D \tan 2\Theta \approx 2D\Theta$ (D, the sample−detector distance), we get $dy_1 \approx R_p\Theta\, d\Theta$ and $dy_2 \approx 2D\, d\Theta$. R_p denotes the Plateau border radius of curvature, constant on the whole concerned surface. We thus obtain $I(y_2) \approx I_0R(y_2/2D)(R_py_2/4D^2)$.

For $\Theta < \Theta_c$, or equivallently $y_2 < 2D\Theta_c \approx 10$ cm, with a typical value $R_p \approx 1$ mm and $R(y_2/2D) \approx 1$, we get a maximal intensity for the spike of the order of $I_{max} = 10^{-6}I_0$, which seems too small. However, at the transition between the flat film and the Plateau border, disjoining pressure effects are still sensible and the radius of curvature may be much larger than the typical Plateau border size, leading to a much larger intensity. Indeed only the very beginning of the Plateau border is seen in this situation. For $\Theta > \Theta_c$, the reflectivity decreases rapidly as $1/\sin^4(\Theta)$, leading to an intensity decreasing as $1/y_2^3$ for $y_2 > 10$ cm. The neutrons deflected in the direction of the spike maximum are coming from the beam sheet $y_1 \approx R_p\Theta_c^2/2 \approx 100$ nm. The film thickness at this point of the Plateau border is thus of the order of $2y_1 \approx 200$ nm, and the Kiessing

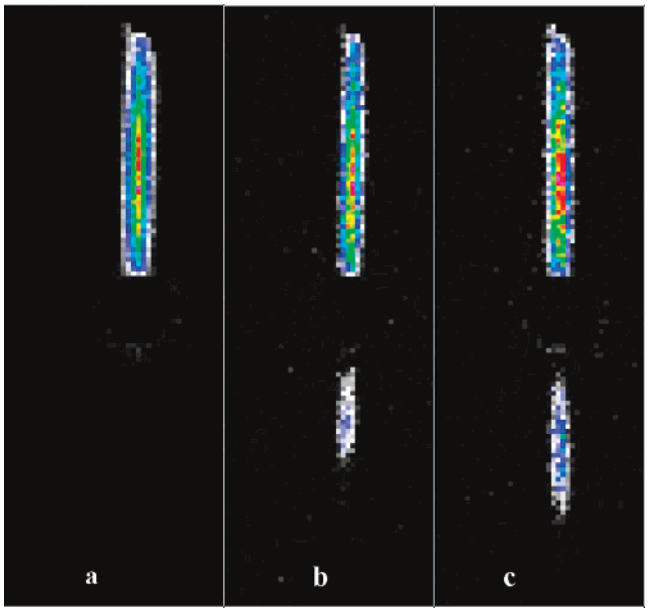

Figure 4. *XY* patterns of the intensity map on the two-dimensional detector (PAXY). The q_0 varies from 0.003 to 0.060 Å^{-1}. In a first step (a), the neutron beam is reflected from the upper film surface. In a second step (b−c), the film is shifted upward by small distances.

fringes are no more observable. Following this, the spike length is then mainly fixed by the angle Θ_c.

Figure 4 shows three patterns of spikes, which might originate from the Plateau borders located at the upper and at the lower sides of the investigated film. To verify the latter assumption, we have used the PAXY spectrometer with better collimation conditions. In particular, the film surface, which was horizontal, was shifted vertically during these measurements (Figure 4). The first observed spike (Figure 4a) only corresponds to the beam reflection on the upper Plateau border. In Figure 4b, the signal below the beamstop is provided by a partial contribution of the lower Plateau border. The last figure illustrates the case of a beam totally reflected by the two Plateau borders. From this short experiment, one can deduce that the contribution of Plateau borders is defined by symmetrical spikes in the diffraction pattern.

In this interpretation, a very small variation of the interface orientation, of the order of Θ_c, can produce spikes. In a real foam, thin films are never completely flat and can thus produce spikes too. The number of spikes due to the presence of the slightly curved thin films can be statistically estimated as follows. In a previous experiment,[8] approximately 25 polyhedral bubbles were hit by the beam, that is, about 175 films as every bubble has

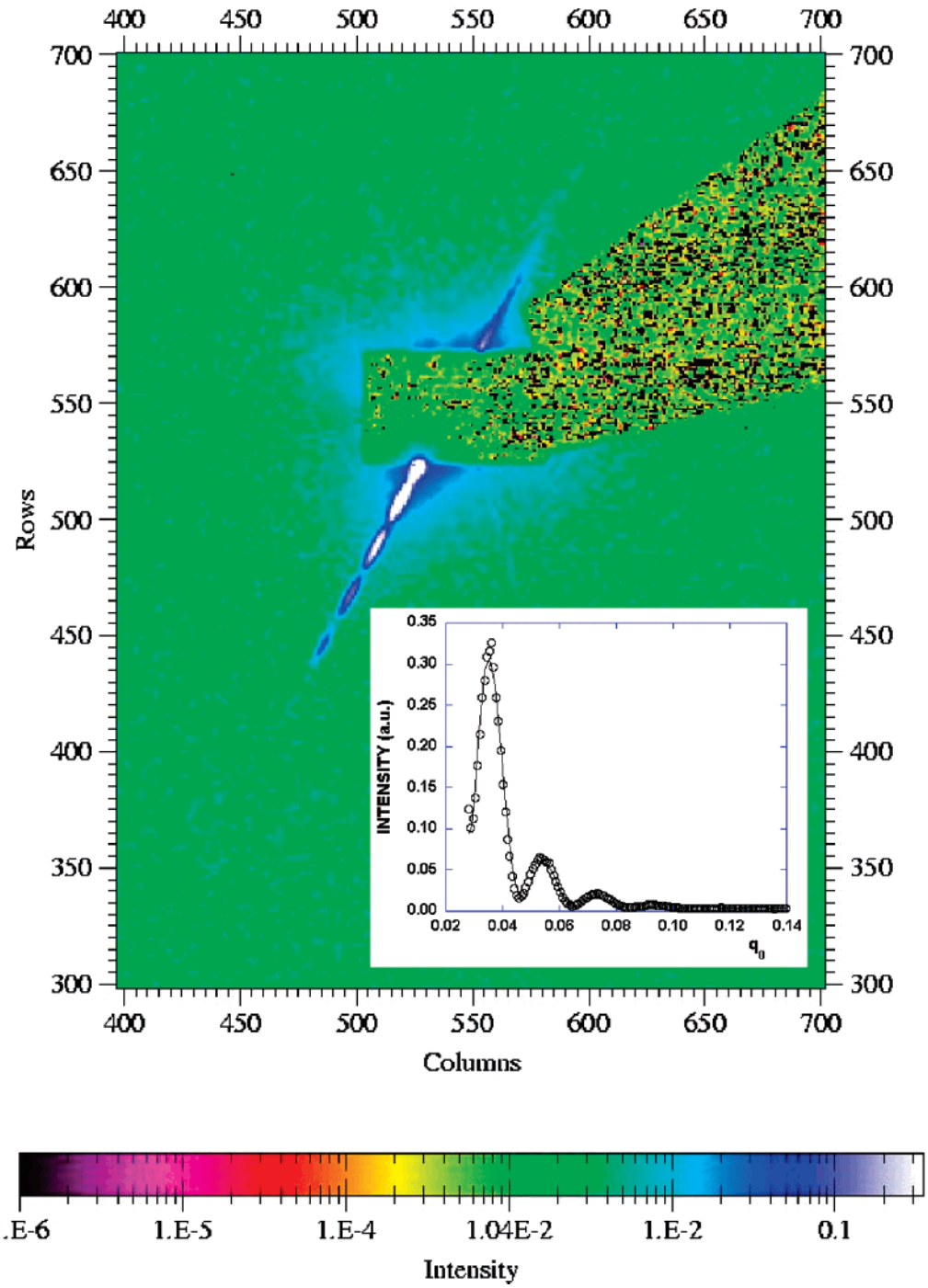

Figure 5. X-ray scattering map (ID2, ESRF). Insert: integrated intensity along the spike (the two-dimensional data have been processed by the FIT2D program); the line passing through the experimental points is a fit using the parameters given in the text.

about between 13 and 14 films on average. To contribute to the observed reflectivity, a film must have its (averaged) normal vector located in a ring of angular aperture 0.01 rad in the plane normal to the beam. The corresponding solid angle is thus $2\pi\Theta_c$. The typical number of reflecting films is thus $175 \times 2\pi\Theta_c/4\pi \approx 1$. The diffraction pattern obtained in this situation has on the order of five spikes, which thus may be explained by the two signatures. The contribution of Plateau borders is more difficult to estimate, because of their complex geometry. They may have a comparable role, but with a different reflectivity function. In a very dry foam, their sizes become very small and they intercept a small part of the beam only. Their contributions may thus become negligible in this case, which is in good agreement with the observation of a spot for a vertical tube, as previously mentionned.

3.3. Thickness of Foam Films. Following eq A.3, spikes due to film curvatures or to Plateau borders should be distinguished by the presence or the absence of intensity oscillations along the spike.

The experimental conditions (exposure time, neutron flux, large incidence angles) were not optimized in these investigations. The incidence angle is related to the film radius whose value increases from a flat surface to a convex one. Consequently, the observed well-defined pattern profile may contain interference fringes. Using the SANS configuration, the value of the parameter q_0 can be estimated from the sample−detector distance D and the

detector dimension (64×64 cm^2): $q_{0\min} \approx (2\pi/\lambda)(3/D)$ and $q_{0\max} \approx (2\pi/\lambda)(32/D)$, giving $q_{0\min} \approx 5.2 \times 10^{-3}$ Å^{-1} and $q_{0\max} \approx 5.6 \times 10^{-2}$ Å^{-1} ($\lambda = 8$ Å, $D = 4.5$ m). Taking into account the average film thickness of SDS/D_2O between 100 and 200 Å,[8] we conclude that the experimental conditions are inadequate to evidence a modulated profile with periodicity 3×10^{-2} or 6×10^{-2} Å^{-1}. However, the main source of uncertainty on the neutron scattering results is in general due to the lack of intensity at high values of q_0 (or angles).

Additional information should be obtained by using X-ray scattering because their energy and their interactions with matter are quite different from those of neutrons. The beam penetration is deeper as indicated by the critical angle which is only around 2.0 mrad. X-rays especially interact with electrons, so that the contrast observed by X-rays is not comparable with neutrons contrast. Experiments performed on real foams produce 2D scattering patterns which are the sum of an isotropic contribution and an anisotropic scattering, called spikes (Figure 5). In the case of SAXS experiments, well-defined oscillations are observed (Figure 5 inset). The spikes are not symmetrical, as expected in the case of grazing incidence SAXS produced by a flat film which is not exactly parallel to the beam. Surprisingly there are some flat films which are enough large to produce well-oriented specular and nonspecular reflectivities. The whole signal is distributed in an angle lower than 1°, and the absence of a well-defined specular reflected beam could be attributed to a huge amplitude of thermally activated fluctuations of the reflection film.[16] Contrary to neutron scattering, the minima and maxima do not scale with the minima and maxima of a $\sin^2(Qd)$ function defined for the simple case of an homogeneous film (eq A.3). The extrema scale better like the one of a $\cos^2(Qd)$ function. The data are well fitted by $[\cos(Qd/2)]^2/Q^4$ (see fit in the Figure 5). The periodicity leads to a distance $d \approx 170$ Å. Such cosinus oscillations are unusual and correspond to the Fourier transform of two planar structures which are identical at the data resolution given by highest Q of the oscillations, e.g., around 60 Å. In this case, the phases of beams are identical after the reflections on both structures, and result in in-phase interferences. The two quasi-identical parallel structures with a mean interdistance of 170 Å in a foam are certainly both air−water interfaces of an unique flat film. The identical phase of the beam after the reflection on both faces demonstrates that these reflections are on an electron density interface with a same sign variation. This is in agreement with a reflection by the sulfate headgroups of the SDS molecules. In situ SAXS experiments of foams offer the unique opportunity to measure the thickness of the few films, which are flat, and their kinetic evolution.

No transition from the common black film to a Newton black film can be detected in the present experiments. But the studied foam appeared as wet with polydisperse bubbles. A synchrotron experiment using a free-draining dry foam with thinner films is planned for understanding the internal structure of the film. Measurements performed in that way could be compared with previous X-ray scattering experiments about free-standing Newton black films.[3−5] In addition, the use of a neutron scattering technique in similar and slightly different prepared foams should provide complementary information (acquisition time, wavevector transfer range, contrast variation, ...), allowing us to explore various geometries and sample environments.

4. Conclusion

SANS investigations from bamboo foams provide in situ information about the structure and the geometry of bubble films. It has been demonstrated that the existence of spikes in anisotropic XY patterns is a signature of the occurrence of specular reflectivity. The position and the elongated shape of a spike provide information about the film orientation with respect to the direction of the incident beam. The observation of a spot is only to be originated to the beam reflection by a thin flat film. The presence of a spike in the diffraction pattern is associated with the curved film or the Plateau border. Oscillations in the reflectivity intensity defined by a Q^{-4} law confirm the film signature from which the thickness can be extracted.

In the near future, we plan to perform time-of-flight investigations to obtain a continuous spectrum of wavelengths. The integrated scattering diffusion should provide accurate information on the internal structure of the film (thickness, molecular organization).

Acknowledgment. We are grateful to G. Le Caer for helpful discussions. We thank S. Bourles and T. Pain for technical assistance.

Appendix: Recall of Basic Specular Reflectivity

From Snell's law the critical glancing angle for total reflection is

$$\sin \Theta_c = \left(\frac{\rho_{liq}}{\pi}\right)^{1/2} \lambda \qquad (A.1)$$

where ρ_{liq} is the scattering length density ($\rho_{liq} \approx \rho_{D_2O} \approx 6.34 \times 10^{10}$ cm^{-2}) and λ is the incident neutron wavelength.

This gives $\Theta_c \approx 0.011$ rad (39′) for SDS-h/D_2O and a wavelength of $\lambda = 8$ Å.

The specular reflection is measured as a function of the wave vector transfer $Q = (4\pi/\lambda) \sin \Theta$. We call Θ the incident angle to the plane of the film (therefore the beam is deflected by an angle $\theta = 2\Theta$, so that in usual small-angle scattering notation, the scattering vector $q = (4\pi/\lambda) \sin \theta/2 = (4\pi/\lambda) \sin \Theta = Q$). The single film consists of two planar air/liquid (here water) interfaces. The phase shifts in the reflectivity profile depend on the path difference between the two interfaces which is determined by d. The ratio between the intensity of the incident beam I_0 and the one $I(\theta)$ reflected by the film is

$$R_F(\Theta) = \frac{I(\Theta)}{I_0} = \frac{(q_0^2 - q_1^2)^2 \sin^2(q_1 d)}{4q_0^2 q_1^2 + (q_0^2 - q_1^2)^2 \sin^2(q_1 d)} \qquad (A.2)$$

where $q_0 = Q/2$ and $q_1^2 = q_0^2 - 4\pi\rho_{liq}$. For $\Theta = \Theta_c$, $R_F(\Theta) \approx q_0^2 d^2/(4 + q_0^2 d^2) \approx Q^2 d^2/(16 + Q^2 d^2)$, which is close to 1 for a thick film ($d \gg 1/Q$) similar to the case of a single interface (Fresnel law). On the contrary, for a thin film ($1/Q \approx d$), $R_F(\Theta)$ decreases as soon as $\Theta > 0$.

In general, if Θ is significantly larger than Θ_c, multiple scattering may be neglected, and the first Born approximation in quantum-mechanical theory becomes valid. For thin film, we are always in this case.

It is easy to reach the large Q regime for which the scattering length density ρ_{liq} for D_2O (neglecting SDS) is small compared to q_0^2, so that $q_1 \approx q_0$. Then, eq A.2 becomes

(15) Guiner, A.; Fournet, G. *Small angle scattering of X-rays*; Wiley: New York, 1955; p 268.

(16) de Jeu, W. H.; Ostrovskii, B. I.; Shalaginov, A. N. *Rev. Mod. Phys.* **2003**, *75*, 181.

$$R_F \approx \frac{\pi {\rho_{liq}}^2 \sin^2(q_0 d)}{{q_0}^4} \propto \frac{\sin^2(Qd/2)}{Q^4} \qquad (A.3)$$

Oscillations of the reflectivity intensity around the Q^{-4} law, the so-called Kiessing fringes, can thus be observed for films of well-defined thickness d.

In such a large Q regime, a Born approximation can be used, under certain conditions, for density profiles $\rho(z)$ more complicated than a simple layer. This gives

$$R(Q) = (4\pi r_e)^2 \frac{1}{\rho_\infty} \left| \int_{-\infty}^{0} \frac{d\rho(z)}{dz} \exp(iQz)\, dz \right|^2 \qquad (A4)$$

Applying eq A.4 to a single layer leads back to expression A.3.

The reflected intensity of a perfect flat film is modified by a Debye−Waller-like factor, considering surface imperfections. If the surface is not entirely smooth, its local roughness modifies the specular reflectivity in a manner similar to that of a diffuse interface[14]

$$R = R_F \exp(-4q_0 q_1 \langle\sigma\rangle^2) \qquad (A.5)$$

where $\langle\sigma\rangle$ is the root-mean-square roughness.

Equation A.5 implies that interface roughness reduces the specularly reflected intensity. The missing intensity is scattered into other (nonspecular) directions. Whereas the specular reflectivity is only sensitive to the structure projected on the surface normal, the nonspecular intensity is sensitive to the in-plane correlations of the interface since it has a nonzero component of the wave vector transfer $\mathbf{Q}$ in the plane. Such spatial fluctuations roughen the surface and the nonspecular reflectivity manifests itself through diffuse scattering. For our SANS experiments, the observed signals have significant intensities and their origin is attributed to the specular reflectivity.

The different expressions given above are valid for a perfect incident beam. The calculated reflectivity must be convoluted with the spectrometer resolution function. For standard reflectivity experiments, the beam angular divergence has two effects: first a decrease of the amplitude of the oscillations (for the interface case), then a rounding of the discontinuity of the reflectivity intensity at the critical angle. To fit data, it is important to have a good knowledge of the beam angular divergence. The angular resolution will be taken into account future experiments.

Equation A.3 is consistent with the SANS intensity calculated for a disk, oriented with an angle Ψ with respect to the incident beam. The form factor $F(q \equiv Q)$ is defined by[15]

$$F(Q) = \left(\frac{\sin((Qd/2)\cos\Psi)}{(Qd/2)\cos\Psi} \frac{2J_1((Qr_d/2)\sin\Psi)}{(Qr_d/2)\sin\Psi} \right)^2 \approx \left(\frac{\sin((Qd/2)\cos\Psi)}{(Qd/2)\cos\Psi} \right)^2 \qquad (A.6)$$

for $Qr_d \gg 1$, since r_d, the radius of the disk is here the one of the diaphragm, $r_d \approx 7$ mm, which makes $J_1(x)$, the first-order Bessel function, identical to 1. Only the sine function oscillates here, around a Q^{-4} decreasing function. Integrating over a uniform distribution of Ψ gives a result proportional to eq A.3.

LA0477338